

Measuring 3D Droplet Shape and local Slope using Interferometry and Continuous Wavelet Transforms

Sam Dehaeck^{1,*}, Yannis Tsoumpas¹, Pierre Colinet¹

¹Transfers, Interfaces and Processes (TIPs) Department, Université Libre de Bruxelles, CP 165/67, Avenue F.D. Roosevelt 50, 1000 Brussels, Belgium.

*corresponding author: sam.dehaeck@gmail.com

Abstract Using Mach-Zehnder interferometry, sufficiently flat transparent objects can be measured with micrometric precision. In the present article, we will detail a novel image processing procedure capable of yielding precise height and local slope information in each pixel, even in the presence of substantial noise. This technique is based on the use of the continuous wavelet transform. A detailed overview of the algorithm will be given and sample results will be discussed.

Keywords: Fringe Analysis, Wavelet Transform, Interferometry

1 Introduction

When studying evaporating droplets, the most important parameters to extract are its volume, contact angle and radius (or wetted surface). Generally, these quantities are extracted from a side-view image and assume axial symmetry of the drop. For the extraction of the contact angle, typically the droplet contour is fitted with a theoretical profile (mostly a simple parabolic profile for sufficiently small droplets) and its slope at the intersection with the substrate is extracted. However, when the contact angle becomes too small (namely $< 10^\circ$) such a side view measurement becomes unreliable. One of the reasons for this is the diffraction coming from the substrate which hinders the contour detection. In such a case, a top view measurement is the best approach. While there are different techniques capable of extracting thickness profiles from a top-view measurement, we will demonstrate here that interferometry is capable of measuring droplets with contact angles up to 20° while maintaining a field of view of 6 by 6mm. As this field of view is large enough to measure typical droplet sizes, we feel that it fills the gap left by the side-view imaging nicely.

While this technique has been around for many years, it is mostly in the image processing part that innovations are continuing to be published capable of giving more precise results in the presence of larger noise levels and in faster processing times. It is also with this objective that the current paper will describe a wavelet-based processing algorithm capable of giving noise-robust results ten times faster than the current state-of-the-art. This algorithm forms the subject of a recent paper by the authors [1].

2 Mach-Zehnder Interferometry

A schematic overview of the set-up is shown in Figure 1(a). A parallel beam coming from a Helium-Neon laser ($\lambda=632.8\text{nm}$) is split in two by a beam splitter. One of these beams then traverses the glass plate and the droplet. Both beams are recombined in the end and the optical path length difference between the two beams leads to interference fringes, which are visualised by the camera. This typically leads to an image such as shown in Figure 1(b). Here, each connected 'line' (black or white) represents a certain height and the height difference between two adjacent lines (of the same colour) is what we will name the 'fringe height' h_f . For a Mach-Zehnder interferometer, we have:

$$h_f = \frac{\lambda}{n-1}$$

with n the refractive index of the liquid and λ the wavelength of the laser. In the present, we will only deal with droplets of Novec-HFE 7100 (from 3M[®]). This liquid evaporates fairly quickly and creates contact angles in the order of 10° . Its refractive index is 1.27 and as such, h_f is equal to $2.26\ \mu\text{m}$. Now in order to obtain a height

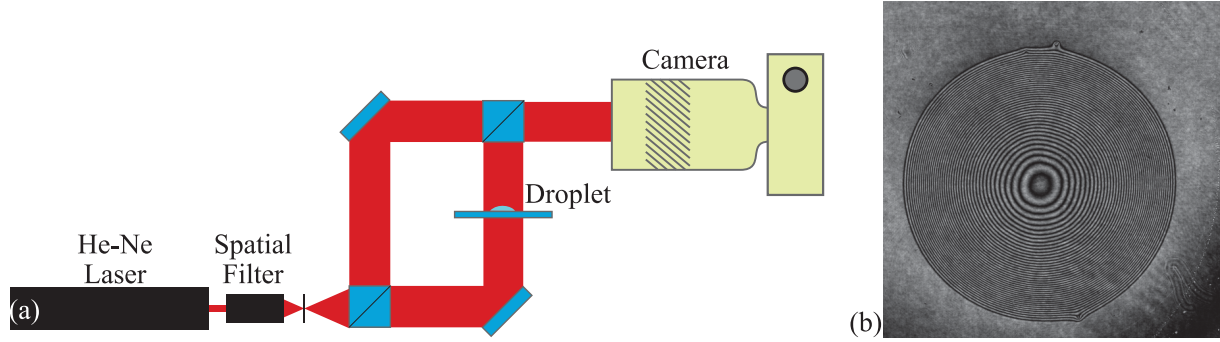


Fig. 1 (a) Experimental Set-Up (b) Typical image of a droplet.

measurement, we need to extract the phase difference ϕ between the two beams. A white region corresponds to constructive interference and hence to a 0 phase difference and black corresponds destructive interference with $\phi = \pi$. However, more advanced image analysis methods will allow us to extract a measure for ϕ in each pixel of the image. With this value, the local height h can then be extracted from its local phase ϕ through:

$$h = \frac{\phi}{2\pi} h_f. \quad (1)$$

It is easy to understand why this technique is limited in maximum contact angles that it can measure. Assuming for convenience that we have a unit magnification objective, we need to make sure that a fringe is imaged onto at least two pixels (Nyquist limit) so that we have at least black-white-black-white. As such, the droplet height can increase no more than 2.26 μm over 6 μm (assuming 3 μm pixels), which corresponds to a maximal angle of 20°. Now obviously using a larger magnification one is able to measure larger angles but this will be at the expense of a smaller field of view. In the above mentioned configuration, a field of view of 6 x 6 mm is nevertheless possible with a 2048 x 2048 camera. This is of course provided that the numerical aperture of the objective is able to accept the refracted ray coming out of the droplet.

3 Algorithm Description

3.1 Introduction

The typical image the algorithm needs to analyse is shown in Figure 1(b). From this single image, it needs to extract the local phase and the local phase gradient which are proportional to the local height and slope respectively. From these two measurements, we can then deduce the drop volume and the contact angle. The main issue encountered is the inherent sign ambiguity present in the phase retrieval; i.e. from a single image it is impossible to determine in which direction the phase is increasing or decreasing. While this problem has been solved many times in literature already, we show here how it can be done with the use of two 2D Fan wavelet transforms. In this way we minimize the amount of directional transforms to only 2, whereas up to 20 were needed before [2].

3.2 Wavelet Ridge Analysis

At the basis of our algorithm is the wavelet ridge phase extraction algorithm and the Fan wavelet. Wavelet ridge analysis is a localised frequency analysis tool in which the signal is compared to wavelets with different frequencies [3]. A typical 2D wavelet used in fringe analysis is the Morlet wavelet. This is a plane wave modulated with a Gaussian window and it is shown in Figure 2(a). In two dimensions it is characterised by two parameters: its scale (or frequency) and its orientation [4]. Cross-correlating the wavelet on the top row of Figure 2(a) with our image, we find the result shown in the right column. Here, the original image was used as a backdrop to better visualise where the cross-correlation plane peaks. As expected, two peaks are visible corresponding to those places where the local frequency and orientation in the image is close to the one of the

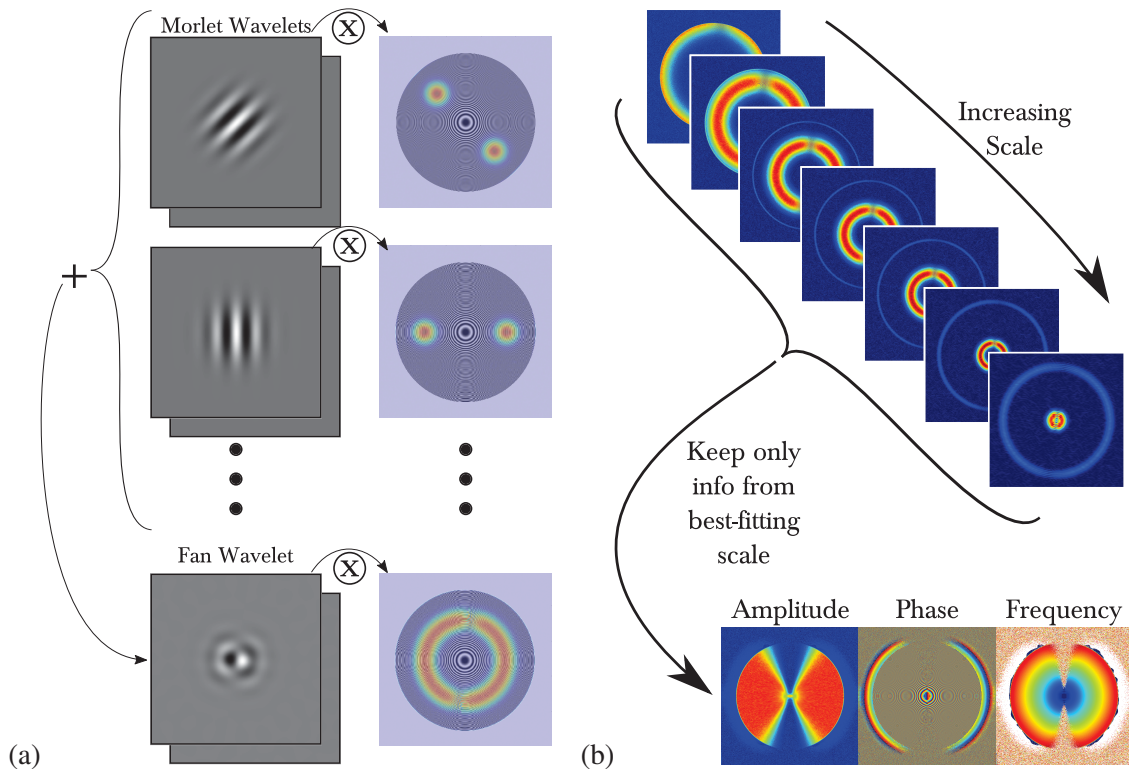


Fig. 2 (a) Morlet versus Fan Wavelet (b) Scanning with different scales.

wavelet. Now, as we are not using a real wavelet but a complex one (with the real part corresponding to a cosine and the imaginary part to a sine) we are also able to get an estimate for the phase in this location, next to the frequency. The obtained phase however, only extends from $-\pi$ to π and a separate processing step called 'phase unwrapping' is needed to get larger phase shifts [5]. To get results for the entire image, we would need to scan over many different orientations and scales (as was done by [2]). However, as we are not interested in the local orientation, we decided to use the so-called Fan wavelet [4, 6, 7] in which several Morlet wavelets are superposed to get a quasi direction insensitive wavelet. As shown in the bottom row, a full ring can now be calculated with a single Fan wavelet. However, this ring still has two small holes on the top and bottom. Thus, a second Fan wavelet with complementary orientations is necessary to get results in the entire image. Nevertheless, using only two Fan wavelets will obviously be 10 times faster than using 20 directional Morlet wavelets [2].

In a second step, different scales need to be explored, which is outlined in Figure 2(b). In the end, we obtain for each Fan wavelet a 3D matrix containing the result of different scales for each pixel. This 3D matrix is then reduced to several 2D matrices by keeping only the information from the best-fitting scale. In this way, we obtain the local amplitude, local phase and also local frequency information. Amplitude and phase is obtained from a module/phase transformation on the complex cross-correlation plane and the frequency comes from the index of the best-fitting scale. The result is shown in the bottom for the 'horizontal' Fan wavelet.

Next step is then to recombine these results with those of the 'vertical' Fan wavelet. This is depicted in Figure 3. This is, as before, based on which of the two results has the largest cross-correlation amplitude with the signal. While this approach works for obtaining the local amplitude and frequency results, for the phase some discontinuity ruins the result. Analysing this further, we find that along a fringe the phase jumps from $-\pi$ to π for no apparent reason. However, as shown in the figure, the absolute value of the phase is obtained correctly. This sign ambiguity problem is related to what was mentioned in the beginning that it is impossible for the computer to know whether the phase is increasing or decreasing. In fact, with respect to the phase result of the horizontal Fan wavelet, the computer always assigns an increase in phase from left to right (due to our underlying choice of Morlet wavelets used in the Fan wavelet). Therefore, what we need to do before the recombination is to flip the sign of the right half so that the phase is decreasing in that part. Similarly, the sign

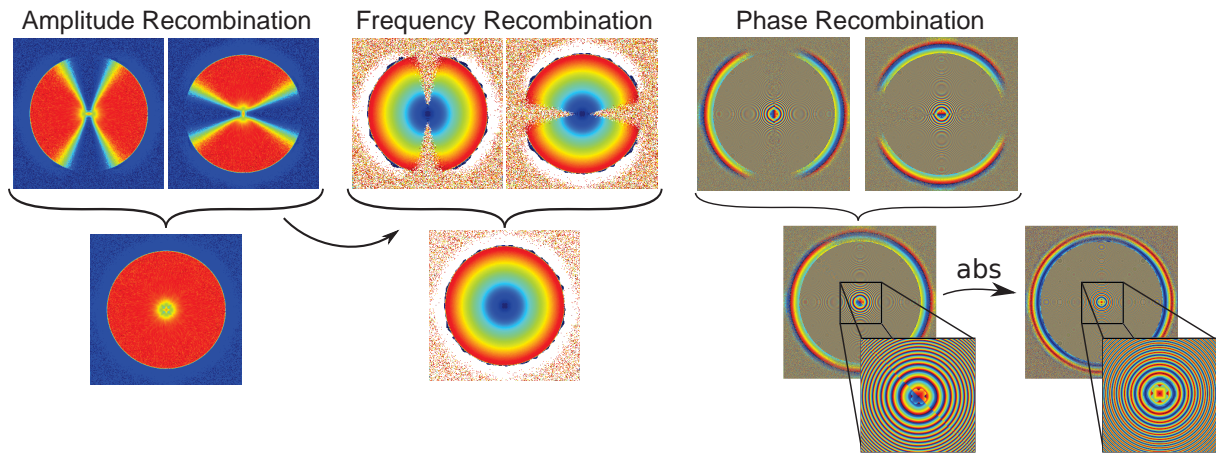


Fig. 3 Recombination of results from horizontal and vertical Fan wavelet.

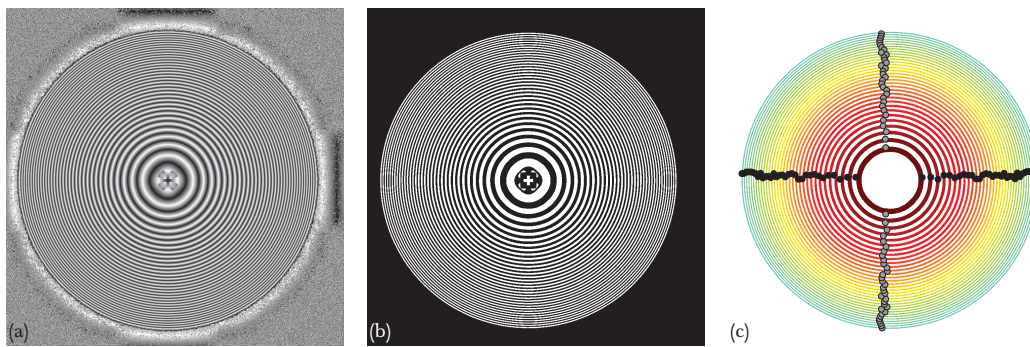


Fig. 4 Skeletonisation-based phase sign flipping (a) Absolute phase map (b) Thresholded absolute phase map (c) Image with all the closed fringes properly labelled and their maximum extents indicated to be used in sign flipping masks.

of the top part of the phase result of the vertical Fan wavelet needs to be changed. A recombination of these modified phase maps now does lead to a consistent phase measurement that gives access to the local height map after unwrapping [5]. The question now of course is how to programmatically select those parts where the sign needs to be flipped. In our paper [1], we describe three different approaches to this problem. We will only briefly go into two of these approaches here.

The simplest approach is based on a skeletonisation of the image and only works for images with a single stagnation point such as Figure 1(b). This is the same problem that we tackled in 2013 using 1D Wavelet transforms [8]. However, the current approach will prove to be many times faster because of the absence of image reinterpolation. The algorithm starts by composing the absolute phase image (i.e. $abs(\phi)$), which can be determined without knowledge of the true sign. From this image (shown in Figure 4(a)), one can now extract (Figure 4(b)) and label some closed fringes (Figure 4(c)). Now, as it turns out, the dividing lines we want to construct go through the 'turning' points of these objects, i.e. the minimal and maximal column and minimal and maximal row extents. Through these points, a parabola is then fitted from which the phase sign flipping masks are easily constructed. From Figure 4(c), all the gray points are thus fitted with a parabola to decide where the sign needs to be flipped in the horizontal phase result and the black dots are used for the vertical result. To demonstrate that this technique is also capable of analysing slightly more complicated images than Figure 1(b), its application on a sliding droplet is shown in Figure 6(b), where the two parabolas are clearly shown.

When the image becomes more complex, a more traditional approach is used, where first the fringe orientation ($0-\pi$) is determined and later transformed into direction ($0-2\pi$). The difference between the two terms is illustrated in Figure 5. This transformation is performed in such a way as to be consistent, namely if the phase on the left side of the image is increasing going towards the center, then it must be decreasing on the right side going towards the edge in order to have the same height in the centre and edge of the droplet. This

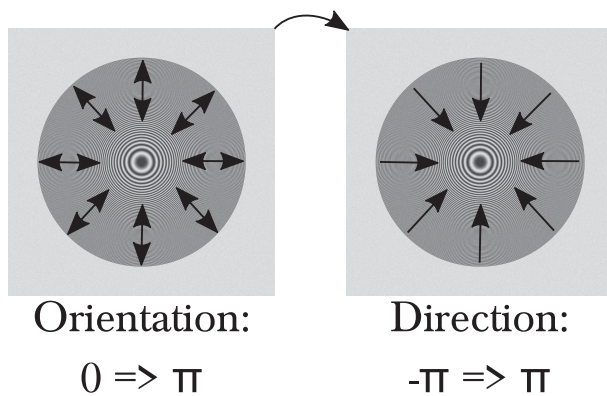


Fig. 5 Orientation versus direction

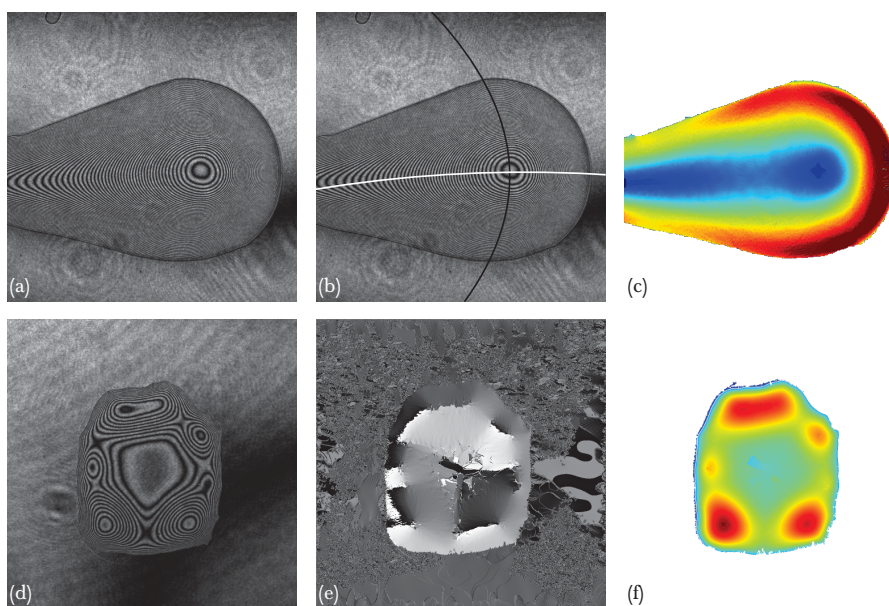


Fig. 6 Some typical applications (reproduced partially from [1]) (a) Image of a sliding droplet (b) Phase sign flipping determined by skeletonisation (c) Local slope image (d) Evaporating ethanol droplet (e) Direction map (f) Local height profile

approach was used for instance in [2] and [9], but also in many articles before that. First step here is obtaining orientational information on the fringes and as mentioned previously, we have sacrificed this ability by the use of the Fan wavelet to gain time. However, what we have access to is a 'noise-free' absolute phase image, which can be used as input for the fast accumulated differences algorithm from [10]. In this way, we get a good orientation map in a fraction of the time with the powerful noise resiliency obtained through the Wavelet transform filtering. The transformation to direction can then be obtained in many ways, here we chose to adapt our phase unwrapping algorithm of choice ([5]) to perform this task as the two problems are very similar. A typical application of this technique to a complicated droplet image is shown in Figure 6(e) where the final direction map is shown. Focusing for instance on the bottom-right 'peak' of the droplet, we see that the direction goes as expected from black ($-\pi$) to white (π) as we circle around this peak. From this direction map, we can then to flip the phase sign for the vertical Fan wavelet when the direction is smaller than zero for instance. In this way, a very precise selection can be made of where to change the sign.

Now, with the phase values properly sorted out, we can move on to the next processing step, which is the 'extraction' of the droplet from the image (i.e. foreground/background segmentation). This is based on the local amplitude image. As seen on the left of Figure 3, the droplet is well contrasted with the background and a simple thresholding will perform the job adequately. The separating line between background and foreground is precisely the contact line. Unwrapping the combined phase result and setting the phase at the contact line

equal to zero (on average), we can transform this to an absolute height map of the droplet with formula 1. Such a height map is shown in Figure 6(f) where multiple maxima in the droplet height profile can be distinguished. From an integration of the local height map, the droplet volume can be calculated. The radius or wetted volume can be found from the segmentation result. Next to this, the local frequency map can also be transformed into a slope image. Such a result is shown in Figure 6(c). Here, one clearly notes how the contact angle is the largest at the leading edge and decreases going towards the trailing edge. For 'normal' droplets such as shown in Figure 1(b), the extraction of the local angle along the contact line pixels will yield a nice Gaussian histogram, from which an accurate measurement of the contact angle can be extracted with a certain uncertainty. And all of the above measurements can be extracted from a single image and therefore can be tracked over time. This is something which can be used in many applications (e.g. [11]). Uncertainty figures for all of these measurements as a function of SNR are described in our paper [1]. For our typical working conditions, the height measurement has typically a precision of about 1/50th of a fringe (i.e. 45 nm) and the volume measurements have an uncertainty of $\pm 1\%$. The local slopes are accurate up to 2%. However, there are two regions of the droplet where the precision is not so good, namely in the centre and at the contact line. In the centre this is due to the fact that the local slope variation during a period becomes too large (phase curvature effects [12]) and at the contact line, this is due to the abrupt truncation of the sinusoidal fringe signal. Neither of these effects has a dramatic influence on our overall results however.

4 Conclusions

Using Mach-Zehnder interferometry, droplets with contact angle ranging up to 20° can be measured in a field of view of 6 x 6 mm. The resulting image can be analysed with a 2D Wavelet Ridge algorithm to treat these closed fringe images. From this, one can extract precise information on local values such as height and slope in each pixel but also global information about contact angle and volume can be tracked over time. On a modern computer, analysing a single image only requires 1.5 seconds.

References

- [1] S. Dehaeck, Y. Tsoumpas, and P. Colinet. Analyzing closed-fringe images using two-dimensional Fan wavelets. *Applied Optics*, 54(10):2939–2952, 2015.
- [2] J. Ma, Z. Wang, B. Pan, T. Hoang, M. Vo, and L. Luu. Two-dimensional continuous wavelet transform for phase determination of complex interferograms. *Applied Optics*, 50(16):2425–2430, 2011.
- [3] P. Tomassini, A. Giulietti, L.A. Gizzi, M. Galimberti, D. Giulietti, M. Borghesi, and O. Willi. Analyzing laser plasma interferograms with a continuous wavelet transform ridge extraction technique: the method. *Applied Optics*, 40(35):6561–6568, 2001.
- [4] J.-P. Antoine and R. Murenzi. Two-dimensional directional wavelets and the scale-angle representation. *Signal Processing*, 52:259–281, 1996.
- [5] M. A. Herraiez, D. R. Burton, M. J. Lalor, and M. A. Gdeisat. A fast two-dimensional phase unwrapping algorithm based on sorting by reliability following a non-continuous path. *Applied Optics*, 41:7437–7444, 2002.
- [6] F. Kirby. Which wavelet best reproduces the fourier power spectrum? *Comput. Geosci.*, 31:846–864, 2005.
- [7] M.A. Gdeisat, D.R. Burton, and M.J. Lalor. Spatial carrier fringe pattern demodulation by use of a two-dimensional continuous wavelet transform. *Applied Optics*, 45(34):8722–8732, 2006.
- [8] S Dehaeck, Y. Tsoumpas, and P. Colinet. Analyzing droplets through digital holography and a 1d wavelet transform technique. In *Digital Holography and Three-Dimensional Imaging*, OSA Technical Digest, page DW3A.5., April 2013.
- [9] Z. Zhang and H. Guo. Fringe phase extraction using windowed fourier transform guided by principal component analysis. *Applied Optics*, 52(27):6804–6812, 2013.
- [10] X. Yang, Q. Yu, and S. Fu. An algorithm for estimating both fringe orientation and fringe density. *Optics Communications*, 274:286–292, 2007.
- [11] Y. Tsoumpas, S. Dehaeck, M. Galvagno, A. Rednikov, H. Ottevaere, U. Thiele, and P. Colinet. Nonequilibrium gibbs criterion for completely wetting volatile liquids. *Langmuir*, 30(40):11847–11852, 2014.
- [12] X. Colonna de Lega. *Processing of non-stationary interference patterns: adapted phase shifting algorithms and wavelet analysis. Application to dynamic deformation measurement by holographic and speckle interferometry*. PhD thesis, Swiss Federal Institute of Technology Lausanne, 1997.